

Experimental implementation of finite-time Carnot cycle

Ruo-Xun Zhai,¹ Fang-Ming Cui,^{1,2} Yu-Han Ma,¹ C. P. Sun,^{1,3,*} and Hui Dong^{1,†}

¹*Graduate School of China Academy of Engineering Physics,
No. 10 Xibeiwang East Road, Haidian District, Beijing, 100193, China*

²*Beijing Normal University, Beijing 100875, China*

³*Beijing Computational Science Research Center, Beijing 100193, China*

(Dated: June 22, 2022)

The Carnot cycle is a prototype of ideal heat engine to draw mechanical energy from the heat flux between two thermal baths with the maximum efficiency, dubbed as the Carnot efficiency η_C . Such efficiency can only be reached by thermodynamical equilibrium processes with infinite time, accompanied unavoidably with vanishing power - energy output per unit time. In real-world applications, the quest to acquire high power leads to an open question whether a fundamental maximum efficiency exists for finite-time heat engines with given power. We experimentally implement a finite-time Carnot cycle with sealed dry air as working substance and verify the existence of a tradeoff relation between power and efficiency. Efficiency up to $(0.524 \pm 0.034)\eta_C$ is reached for the engine to generate the maximum power, consistent with the theoretical prediction $\eta_C/2$. Our results shall provide a new platform for studying finite-time thermodynamics consisting of nonequilibrium processes.

Heat engine is a major machinery to convert heat into the useful energy, such as mechanic work or electricity. Sadi Carnot derived in 1824 an upper bound $\eta_C = 1 - T_c/T_h$ [1, 2] for the conversion efficiency from heat to useful energy in the Carnot cycle with two isothermal processes with the working substance in two thermal baths with temperatures T_c and T_h and two adiabatic processes. In isothermal processes, a control parameter is tuned in a quasi-static fashion - physically much slower than the equilibrium time scale - to reach the Carnot efficiency [2]. Faster processes typically result in more energy dissipation with a consequently lower efficiency, yet can potentially increase the output power [3]. Such tradeoff between power and efficiency suggests the possibility to thermodynamically optimize the two, e.g. increasing efficiency while retaining the power or vice versa [4–10]. One might wonder what is the best achievable efficiency, if exists, for any output power posted by the fundamental laws of thermodynamics [11–13].

Answering such question requires the quantitative evaluation of irreversibility in the fundamental non-equilibrium thermodynamics [14, 15]. Theoretical models near equilibrium were explored recently to reveal a tradeoff relation between power and efficiency [11–13, 16, 17]. More importantly, a fundamental limit of efficiency with a leading order $\eta_C/2$ is predicted for the engine generating the maximum power [7, 9, 10, 18]. Aside from the theoretical achievements, it remains with urgency to devise finite-time heat engine cycles to experimentally test the fundamental finite-time thermodynamical constraints [19–21]. The current main difficulty to implement a finite-time Carnot cycle is to promptly change the temperature of the thermal bath before and after the adiabatic processes, whose duration is far shorter than the equilibrium time to avoid heat exchange [20]. We develop an adiabatic-without-run scheme to implement the finite-

time Carnot cycle by separately running only two isothermal processes in the high- and low-temperature baths. Without actual run of the two adiabatic processes, we can change the bath temperature with the desired accuracy to evaluate the performance of the finite-time Carnot engine. Our scheme allows all the essential quantities for evaluating the engine's performance to be obtained by the directly measurable work in the two isothermal processes with the first law of thermodynamics of energy conservation.

We present an experimental verification of the power-efficiency tradeoff relation with the dry air as working substance in the finite-time Carnot cycle, which is implemented by changing the gas volume $V(t) = V_0 + \mathcal{A}L(t)$ via moving a piston along a designed path $L(t)$. $\mathcal{A} = \pi d^2/4$ is the area of the cross section of the cylindric chamber with the diameter $d = 5.00\text{cm}$. We trace the pressure $p(t)$ with pressure sensors on the chamber. The maintenance of the bath temperature ($\pm 0.1\text{K}$) is achieved by a designed water tank equipped with the feedback temperature control unit.

The Clapeyron pressure-volume (p - V) graph is shown in Fig. 1a with two finite-time isothermal processes (red and blue curves) and two no-run adiabatic processes (green curves). In each run, the system is immersed in the water bath for 10 seconds to allow the initial equilibration of the gas system with the water bath. And the gas is expanded (red line $A \rightarrow B'$ in Fig. 1b) or compressed (blue line $C \rightarrow D'$ in Fig. 1c) in the two isothermal processes with constant speeds controlled by a step motor with the precision $\pm 0.02\text{mm}$. The pressure traces $p(t)$ (red and blue curves) measured in the two processes deviates significantly from the equilibrium pressure (dashed black curve) due to the finite relaxation time $\tau_{\text{relax}} = 2.77\text{s}$. After the expansion and compression, additional waiting time ($2\tau_{\text{relax}}$) is added to allow

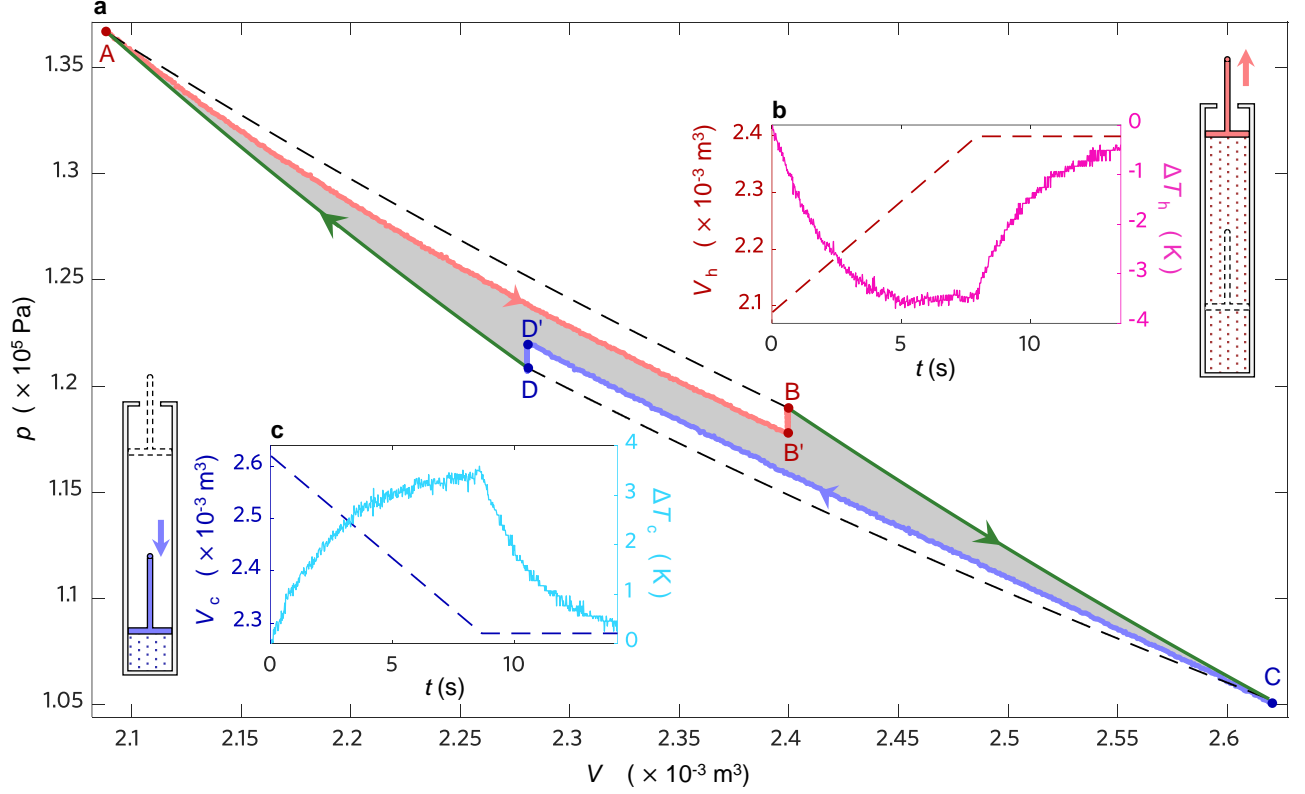


Figure 1. The finite-time Carnot cycle under the temperature combination $(T_h, T_c) = (319.2, 308.2)$ K. a. The Clapeyron pressure-volume ($p-V$) graph of the finite-time Carnot cycle. The red and blue lines show the finite-time isothermal expansion ($A \rightarrow B' \rightarrow B$) with duration τ_h and compression ($C \rightarrow C' \rightarrow D$) with duration τ_c , and the green lines show the adiabatic processes ($B \rightarrow C$ and $D \rightarrow A$) without actual run. Two relaxation processes ($B' \rightarrow B$ and $D' \rightarrow D$) with the waiting time $2\tau_{\text{relax}}$ are added to allow the system to reach the equilibrium with the thermal bath. The ideal Carnot cycle ($A \rightarrow B \rightarrow C \rightarrow D$) is presented as the gray dashed lines for reference. b-c. The gaseous volume $V_{h(c)}(t)$ and the effective temperature trace $\Delta T_{h(c)}(t)$ during the finite-time isothermal expansion and compression. The ideal gas is expanded or compressed with the constant speed $L(t) = L_0 + \nu t$, with $\nu_{\text{exp}} = 20.00$ mm/s and $\nu_{\text{com}} = 20.00$ mm/s. The total time for the example cycle is $t_{\text{tot}} = 25.92$ s.

the gas relaxing to the equilibrium state ($B' \rightarrow B$ and $D' \rightarrow D$). The four piston positions (A, B, C, D) are designed (see supplementary materials) for each temperature combination (T_h, T_c) to ensure the connection between the end (B and D) of one finite-time isothermal process to the beginning (C and A) of the other one with adiabatic processes. We run the engine cycles with 10 temperature combinations to span the Carnot efficiency from $\eta_C = 0.0063$ with the temperature combination $(313.2, 311.2)$ K to $\eta_C = 0.0343$ with $(319.2, 308.2)$ K.

To evaluate the performance (power and efficiency) of the designed cycle, we calculate the work performed in each process with the integral $W(t) = -\int p(t) dL(t)$. The heat exchange is obtained with the conservation of energy as $\Delta Q = -W + \Delta U$, where ΔU is the internal energy change of the gas. The important properties of the ideal gas is that its internal energy depends only on its temperature T_s , which is experimentally determined by the ideal gas law via the state equation $pV = nRT_s$ with the amount of substance of gas in moles n and the

ideal gas constant R . The temperature deviations from the thermal bath $\Delta T_{h(c)}(t) = T_s(t) - T_{h(c)}$ are illustrated with solid lines (cyan and purple) in Fig. 1b and 1c. The relaxation processes at the end of each isothermal process ensure the unchanged internal energy $\Delta U_{A \rightarrow B} = \Delta U_{C \rightarrow D} = 0$, since the gas is nearly in equilibrium with the water bath $\Delta T_{h(c)}(t) \approx 0$. The heat absorbed from the high(low)-temperature bath is measured directly via

$$Q_{h(c)} = -W_{h(c)} = \int_0^{\tau_{h(c)}} p(t) A \dot{L}(t) dt, \quad (1)$$

where τ_h (τ_c) is the operation time for the isothermal expansion (compression) process $A \rightarrow B' \rightarrow B$ ($C \rightarrow D' \rightarrow D$). The total work extracted W_{tot} of the whole cycle is measured by the difference of heat exchanges, $W_{\text{tot}} = Q_h + Q_c$. And the power is calculated as the total work extracted during a cycle divided by the total duration of the cycle, $P(\tau_h, \tau_c) = W_{\text{tot}}/(\tau_h + \tau_c)$. The efficiency is given by the ratio between the extracted work W_{tot} and the input heat Q_h from the high-temperature

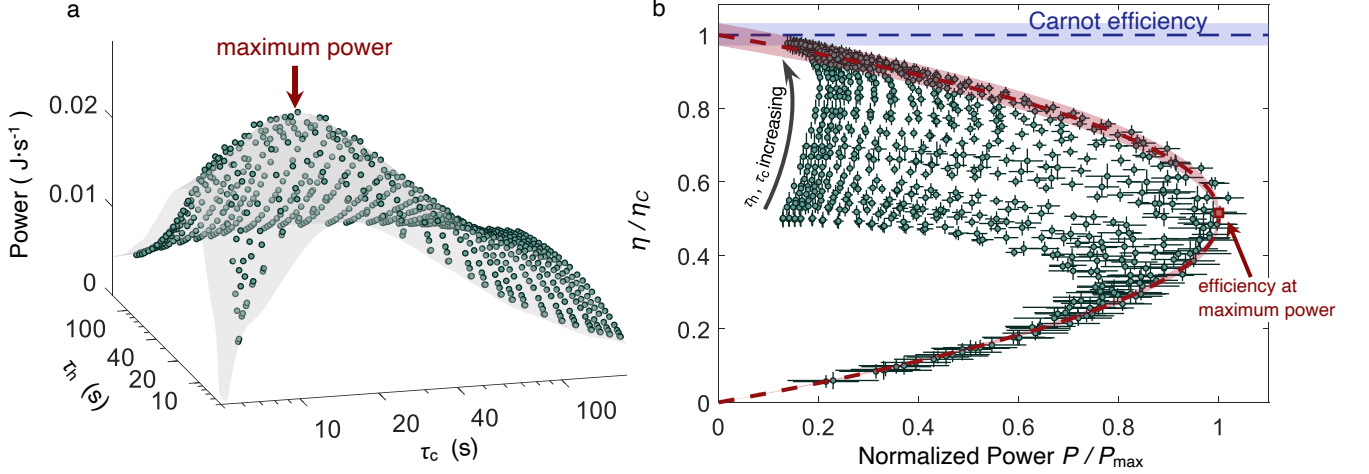


Figure 2. Power and efficiency of the finite-time Carnot engine under the temperature combination $(T_h, T_c) = (319.2.0, 308.2)\text{K}$. a. Output power $P(\tau_h, \tau_c)$ as a function of operation time (τ_h, τ_c) . Each blue circle shows the output power averaged over 8 repeats of the measurement. The arrow shows the position of the maximum power with the control time $\tau_h^* = 13.32\text{s}$ and $\tau_c^* = 12.60\text{s}$. b. Efficiency-power tradeoff (blue circles with error bar). The dashed green curve shows the Carnot efficiency $\eta_C = 0.0343$, and the blue shadow presents the efficiency fluctuation due to temperature variation of the water bath during the experiments. The dashed red line shows the theoretical constraint [13] between the normalized efficiency $\tilde{\eta} \equiv \eta/\eta_C$ and power $\tilde{P} \equiv P/P_{\max}$ with the upper bound $\tilde{\eta} \leq 1 - (1 - \eta_C) \tilde{P}/[2(1 + \sqrt{1 - \tilde{P}}) - \eta_C \tilde{P}]$ and the lower bound $\tilde{\eta} \geq 1 - \sqrt{1 - \tilde{P}}$ with the temperature fluctuation represented by the red shadow.

thermal bath, $\eta(\tau_h, \tau_c) = W_{\text{tot}}/Q_h$. In Fig. 2a, we show how the power $P(\tau_h, \tau_c)$ changes with the two operation time τ_h and τ_c for one cycle under the temperature combination $(T_h, T_c) = (319.2.0, 308.2)\text{K}$. The competition between the increase of work (equals to the gray area enclosed by the $p - V$ curve) and the increase of operation time results in the maximum power $P_{\max} = 0.030\text{J} \cdot \text{s}^{-1}$ on the power surface with the control time $\tau_h^* = 13.32\text{s}$ and $\tau_c^* = 12.60\text{s}$ (red arrow in Fig. 2a).

Recently, much attentions are drawn to find the trade-off between power and efficiency for finite-time thermodynamic cycles, e.g., Carnot cycle [7, 20]. Within the framework of the low-dissipation model [7, 9], a power and efficiency tradeoff relation [11–13] is predicted for finite-time Carnot cycle. Figure 2b shows the scatter plot of the normalized efficiency η/η_C and the normalized output power P/P_{\max} for cycles with changing operation time τ_h and τ_c . The error bars of each set P and η are obtained from 8 repeats of the experimental runs. The experimental data fall into the region enclosed by two margins of maximum and minimum efficiencies, which are illustrated as red dashed line with a red shadow area reflecting the fluctuation of the bath temperature in Fig. 2b. The data illustrates not only an upper bound for the achievable efficiency, but also a lower bound for the worst efficiency for the current finite-time Carnot cycle. The cycle achieves the Carnot efficiency $\eta_C = 0.0343$ with the increasing operation time τ_c and τ_h at the top left corner with a vanishing power.

The key quantity to evaluate the finite-time Carnot

cycle is the efficiency at the maximum power η_{EMP} , which was suggested as a physical efficiency limit independent of the properties of the working substance [5, 9]. We extract the efficiency at the maximum power η_{EMP} for all the temperature combinations in our experiment, and show its dependence on the Carnot efficiency in Fig. 3a. The obtained maximum efficiencies (markers with error bars) follow a simple relation $\eta_{\text{EMP}} = (0.524 \pm 0.034)\eta_C + \mathcal{O}(\eta_C^2)$, which agrees well with the Curzon-Ahlborn efficiency [5] $\eta_{\text{CA}} = 1 - \sqrt{1 - \eta_C}$ and the recent proposed bound [8, 9] $\eta_C/(2 - \eta_C)$ to the first order of the Carnot efficiency η_C as $\eta_{\text{EMP}} = \eta_C/2 + \mathcal{O}(\eta_C^2)$. The coefficient 1/2 was proved as a universal value independent of the system-specific features in the linear response regime due to the symmetry of the Onsager relations [7, 15]. Our experimental data provides the first demonstration of the leading order with the coefficient 1/2.

The optimization of the cycle for maximum power is achieved by choosing the operation time τ_h and τ_c . We determine the corresponding optimal operation time (τ_h^*, τ_c^*) (markers in Fig. 3b) to reach the maximum power for cycles with all temperature combinations in the current experiment. The optimal time (τ_h^*, τ_c^*) is verified to be in the regime where the $1/\tau$ scaling is valid [20, 22] (discussions in the supporting materials). With higher Carnot efficiency, less optimal operation time is needed to achieve the maximum efficiency and in turn more irreversibility is generated.

We have experimentally implemented the finite-time

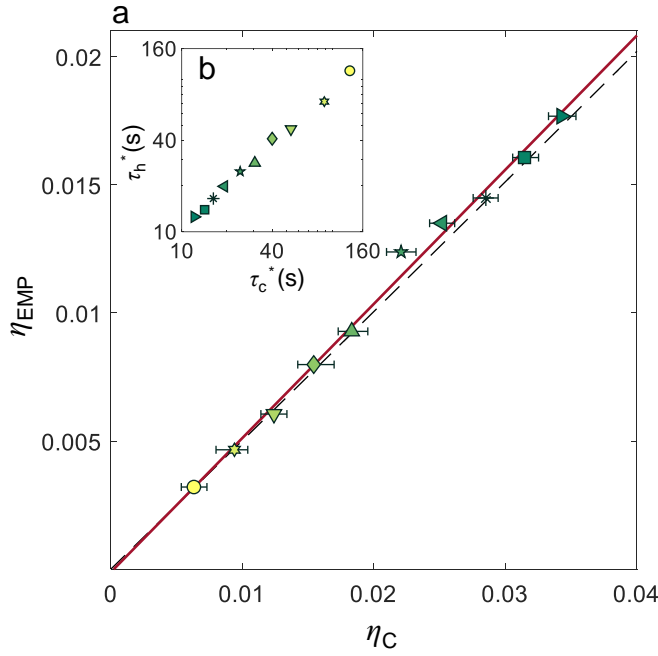


Figure 3. Optimized finite-time Carnot cycle with maximum power. a. Efficiency at maximum power (markers with error bars) as a function of Carnot efficiency. The red solid line shows the linear fit $\eta_{\text{EMP}} = a + b\eta_C$ yielding the parameters $a = \pm 7.0 \times 10^{-4}$ and $b = 0.524 \pm 0.034$. The dashed black line shows the Curzon-Ahlborn efficiency $\eta_{\text{CA}} = 1 - \sqrt{1 - \eta_C}$. b. Optimal operation time (τ_h^*, τ_c^*) for the maximum power in the cycles with different Carnot efficiencies.

Carnot cycle with the dry air as working substance. For any given output power, we have shown the existence of the highest efficiency achieved with the designed operation time. Our results verify the existence of a universal relation of the efficiency at maximum power $\eta_{\text{EMP}} = \eta_C/2 + \mathcal{O}(\eta_C^2)$ to the first order of the Carnot efficiency. We believe that our work will spur more experimental efforts into explore the finite-time thermodynamics.

This work is supported by the National Natural Science Foundation of China (NSFC) (Grants No. 12088101, No. 11534002, No. 11875049, No. U1930402, No. U1930403 and No. 12047549) and the National Basic Research Program of China (Grant No. 2016YFA0301201).

* cpsun@gscaep.ac.cn

† hdong@gscaep.ac.cn

[1] Carnot, S. *Reflections on the Motive Power of Heat and*

on Machines Fitted to Develop that Power (J. Wiley, 1890).

- [2] Callen, H. B. *Thermodynamics and an Introduction to Thermostatistics* (John Wiley & Sons, 1985).
- [3] Andresen, B., Salamon, P. & Berry, R. S. Thermodynamics in finite time. *Physics today* **63** (1984).
- [4] Novikov, I. The efficiency of atomic power stations. *J. Nucl. Energy* **7**, 125–128 (1958).
- [5] Curzon, F. L. & Ahlborn, B. Efficiency of a carnot engine at maximum power output. *Am. J. Phys.* **43**, 22–24 (1975).
- [6] Andresen, B., Berry, R. S., Nitzan, A. & Salamon, P. Thermodynamics in finite time. i. the step-carnot cycle. *Phys. Rev. A* **15**, 2086–2093 (1977).
- [7] Van den Broeck, C. Introduction to thermodynamics of irreversible processes. *Phys. Rev. Lett.* **95**, 190602 (2005).
- [8] Schmiedl, T. & Seifert, U. Efficiency at maximum power: An analytically solvable model for stochastic heat engines. *EPL (Europhysics Letters)* **81**, 20003 (2007).
- [9] Esposito, M., Kawai, R., Lindenberg, K. & Van den Broeck, C. Efficiency at maximum power of low-dissipation carnot engines. *Phys. Rev. Lett.* **105**, 150603 (2010).
- [10] Tu, Z. C. Efficiency at maximum power of feynman's ratchet as a heat engine. *J. Phys. A: Math. Theor.* **41**, 312003 (2008).
- [11] Ryabov, A. & Holubec, V. Maximum efficiency of steady-state heat engines at arbitrary power. *Phys. Rev. E* **93**, 050101 (2016).
- [12] Shiraishi, N., Saito, K. & Tasaki, H. Universal trade-off relation between power and efficiency for heat engines. *Phys. Rev. Lett.* **117**, 190601 (2016).
- [13] Ma, Y.-H., Xu, D., Dong, H. & Sun, C.-P. Universal constraint for efficiency and power of a low-dissipation heat engine. *Phys. Rev. E* **98**, 042112 (2018).
- [14] Prigogine, I. *Introduction to the Thermodynamics of Irreversible Processes* (Wiley, 1968), 3rd edition edn.
- [15] Seifert, U. Stochastic thermodynamics, fluctuation theorems and molecular machines. *Rep. Prog. Phys.* **75**, 126001 (2012).
- [16] Chen, L. & Yan, Z. The effect of heat-transfer law on performance of a two-heat-source endoreversible cycle. *J. Chem. Phys.* **90**, 3740–3743 (1989).
- [17] Chen, Y. H., Chen, J.-F., Fei, Z. & Quan, H. T. A microscopic theory of curzon-ahlborn heat engine. *arXiv* (2021).
- [18] Holubec, V. & Ryabov, A. Maximum efficiency of low-dissipation heat engines at arbitrary power. *J. Stat. Mech.: Theory E.* **2016**, 073204 (2016).
- [19] Blickle, V. & Bechinger, C. Realization of a micrometre-sized stochastic heat engine. *Nat. Phys.* **8**, 143–146 (2011).
- [20] Martínez, I. A. *et al.* Brownian carnot engine. *Nat. Phys.* **12**, 67–70 (2015).
- [21] Rossmagel, J. *et al.* A single-atom heat engine. *Science* **352**, 325–329 (2016).
- [22] Ma, Y.-H., Zhai, R.-X., Chen, J., Sun, C. P. & Dong, H. Experimental test of the 1/t-scaling entropy generation in finite-time thermodynamics. *Phys. Rev. Lett.* **125**, 210601 (2020).

Supplementary material for “Experimental implementation of finite-time Carnot cycle”

Ruo-Xun Zhai,¹ Fang-Ming Cui,^{1,2} Yu-Han Ma,¹ C. P. Sun,^{1,3,*} and Hui Dong^{1,†}

¹Graduate School of China Academy of Engineering Physics, Beijing 100193, China

²Beijing Normal University, Beijing 100875 China

³Beijing Computational Science Research Center, Beijing 100193, China

(Dated: June 22, 2022)

I. EXPERIMENTAL APPARATUS - CALIBRATION OF THE CYLINDRIC VOLUME

Experimental setup. The sealed dry air is prepared as the work substance for the finite-time Carnot cycle. The dry detergent (CaCl_2) is placed in the chamber before sealed with the silicon grease to avoid gas leakage. The chamber (homebuilt) is set for 24 hours to allow the absorption of the moisture in the sealed air. The water bath ($\sim 0.1\text{m}^3$) is circulated with a water pump to ensure the uniform temperature distribution in the water bath. Before each sets of finite-time Carnot cycles, the water temperature is firstly raised to the desired degree ($\pm 0.1\text{K}$). And the chamber is then immersed for 30 minutes in the bath to allow the initial equilibrium with the water bath.

Three pressure sensors measure the absolute pressure with the range (0-0.15MPa) and the precision 0.2% F.S (300Pa). The position sensor measures the piston displacement with the range (0mm- 300.00mm). The obtained data is used to synchronize the position data from stepper motor. The temperature sensor (PT100) with the precision 0.1K is used to monitor the temperature of water bath. The data acquisition is through collecting the current (4-20mA) at the frequency of 50Hz.

The piston is controlled by the stepper motor with the maximum speed $v_{\max} = 150.00\text{mm/s}$ and maximum acceleration $a_{\max} = 400.00\text{mm/s}^2$. The total time $\tau = \Delta L/v + v/a_{\max} + 2\tau_{\text{relax}}$ is archived with the designed speed v to move the piston by the displacement ΔL .

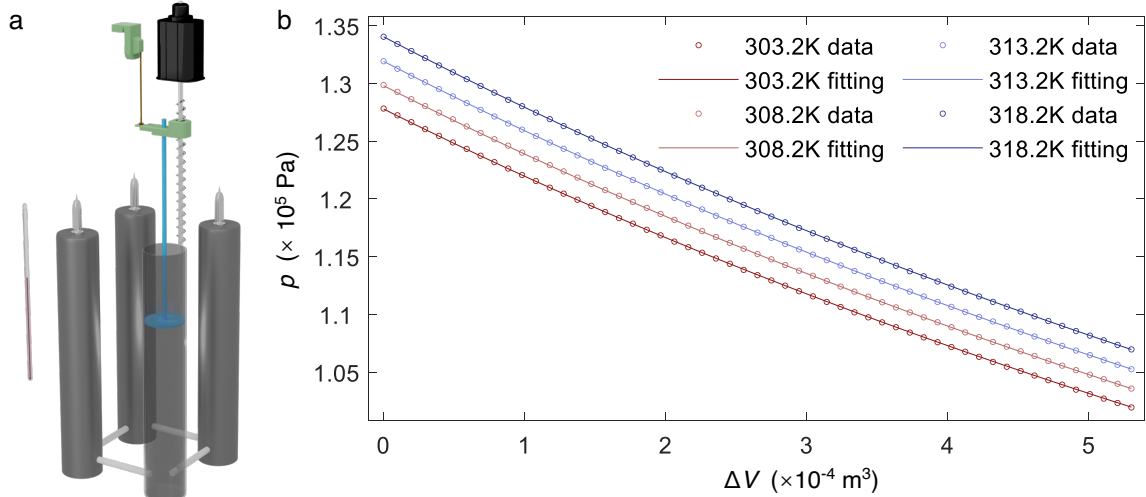


FIG. S1. The experimental setup and the volume calibration. a. The experimental setup. b. Fitting of ideal gas law to obtain the amount of substance n and the volume V_{\min} . We measured ΔV together with p when the bath is at 303.2K, 308.2K, 313.2K, and 318.2K. The fitting of the data with $p(V_{\min} + \Delta V) = nRT$ yields $V_{\min} = 2.094 \times 10^{-3}\text{m}^3$, $n = 0.1062\text{mol}$.

The design of the chamber (diameter $d = 5.00\text{cm}$) is illustrated in Figure S1(a). With the area of the piston section $\mathcal{A} = \pi d^2/4 = 1.963 \times 10^{-3}\text{m}^2$, we measure the gas volume change $\Delta V = \mathcal{A}\Delta L \equiv V - V_{\min}$ with ΔL as the displacement of stepper motor. The unknown volume V_{\min} is calibrated with the state function of the ideal gas

$$p(V_{\min} + \mathcal{A}\Delta L) = nRT, \quad (\text{S1})$$

where p , ΔL and T are measured with sensors. Here $R = 8.3145\text{J} \cdot \text{K}^{-1} \cdot \text{mol}^{-1}$ is the ideal gas constant, and n is the amount of substance. For one temperature, we measured the pressure p as a function of the displacement ΔL . The

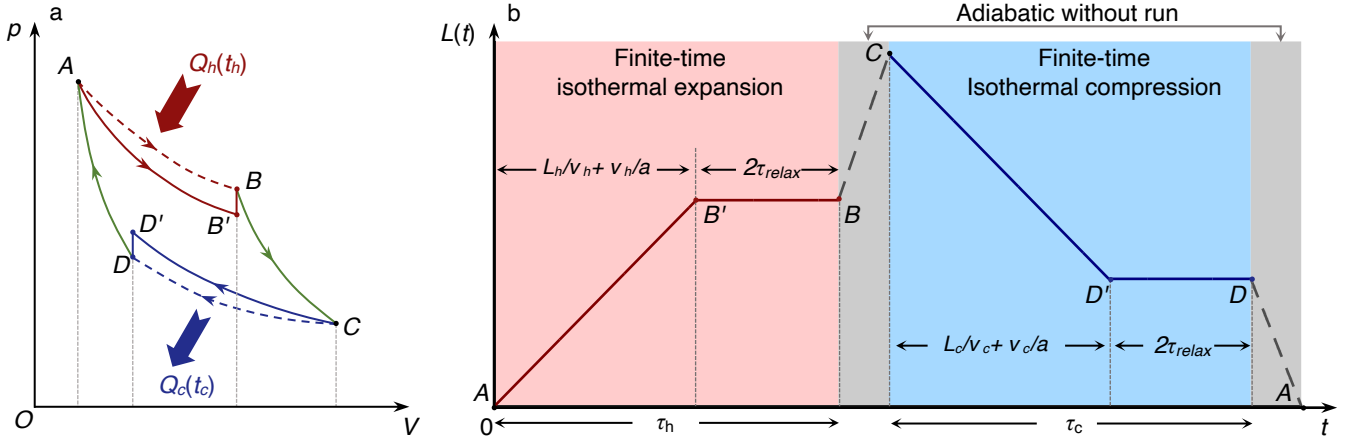


FIG. S2. Diagram of finite-time Carnot cycle in our adiabatic-without-run scheme and the piston position $L(t)$. (a) The Clapeyron pressure-volume ($p(t) - V(t)$) diagram. (b) The designed piston movement $L(t)$ for the cycle.

piston is moved to one position and set for 30 seconds to allow the equilibrium in order to acquire the pressure data $p(\Delta L)$. The data for the pressure p as a function of $\Delta V = \mathcal{A}\Delta L$ is illustrated in Fig. S1 for different temperatures 303.2K, 308.2K, 313.2K, and 318.2K. And the volume V_{\min} and n are treated as two fitting parameters. The fitting of Eq.S1 yields $V_{\min} = 2.094 \times 10^{-3} \text{m}^3$, $n = 0.1062 \text{mol}$. The volume is then explicitly expressed as function of the displacement of the piston ΔL as

$$V = 1.963 \times 10^{-3} \text{m}^3 \times \Delta L + 2.094 \times 10^{-3} \text{m}^3. \quad (\text{S2})$$

II. FINITE-TIME CARNOT CYCLE DESIGN

Our design of the adiabatic-without-run scheme is illustrated in Figure S2. The key ideal is to complete the finite-time Carnot cycle with only running two finite-time isothermal processes and without running the two adiabatic processes. Such design is based on the fact that the evaluation of the finite-time Carnot cycle is through the two experimentally measured quantities, the total work extracted and the total time of the cycle. The total work extracted $W_{\text{tot}} = Q_h + Q_c$ is obtained by the difference of the heat exchange during the finite-time isothermal expansion (Q_h) and compression process (Q_c) with the help of the first law of thermodynamics - energy conservation. Therefore there is no need to actually run the two adiabatic processes to obtain the total work. In term of the total cycle time, the operation of adiabatic process requires short operation time (shorter than the relaxation time τ_{relax}) to avoid heat exchange. The time for adiabatic processes are neglected in our experiments as well as in the theoretical works [1, 2].

Experimental protocol. To complete the cycle in our adiabatic-without-run scheme, we have to ensure the connection between the end of one finite-time isothermal process to the beginning of the other one with an adiabatic process via the following equations

$$\begin{aligned} V_B^{\gamma-1} T_h &= V_C^{\gamma-1} T_c, \\ V_D^{\gamma-1} T_c &= V_A^{\gamma-1} T_h, \end{aligned} \quad (\text{S3})$$

where γ is the ratio between specific heats at constant pressure and at constant volume ($\gamma = 1.40$ for the dry air [3]). The additional relaxation processes with the duration $2\tau_{\text{relax}}$ are added to allow the equilibrium with the thermal bath. The minimum of the volume V_{\min} is reached with $L_A = 0$, and the maximum volume V_C is reached at $L_C = 270.00 \text{mm}$. The sets of the designed connection points L_i ($i = B, D$) are calculated with the connection condition in Eq. (S3) and presented in Table S1.

$T_h(K)$	$T_c(K)$	η_C	Finite-time isothermal expansion		Finite-time isothermal compression	
			$L_A(mm)$	$L_B(mm)$	$L_C(mm)$	$L_D(mm)$
313.2	311.2	6.39×10^{-3}	0	248.76	270.00	17.22
313.2	310.2	9.58×10^{-3}	0	238.22	270.00	25.98
314.2	310.2	12.73×10^{-3}	0	227.86	270.00	34.72
315.2	310.2	15.87×10^{-3}	0	217.62	270.00	43.50
316.2	310.2	18.98×10^{-3}	0	207.49	270.00	52.33
317.2	310.2	22.07×10^{-3}	0	197.47	270.00	61.20
317.2	309.2	25.22×10^{-3}	0	187.31	270.00	70.34
318.2	309.2	28.29×10^{-3}	0	177.48	270.00	79.32
319.2	309.2	31.33×10^{-3}	0	167.76	270.00	88.34
319.2	308.2	34.47×10^{-3}	0	157.80	270.00	97.74

TABLE S1. Table for the piston positions of finite-time Carnot cycle. The piston position B and D are calculated with Eq. (S3).

For each cycle, 27 different values of speeds (v_h and v_c) are chosen to achieve the series of control time set τ_h and τ_c for finite-time isothermal expansion and compression processes. The value of these speeds v are 150.00, 120.00, 100.00, 80.00, 60.00, 40.00, 30.00, 24.00, 20.00, 15.00, 12.00, 10.00, 8.00, 6.00, 5.00, 4.00, 3.50, 3.00, 2.70, 2.40, 2.00, 1.70, 1.50, 1.30, 1.20, 1.10, and 1.00 mm/s. For each speed, the process are repeated for 8 times.

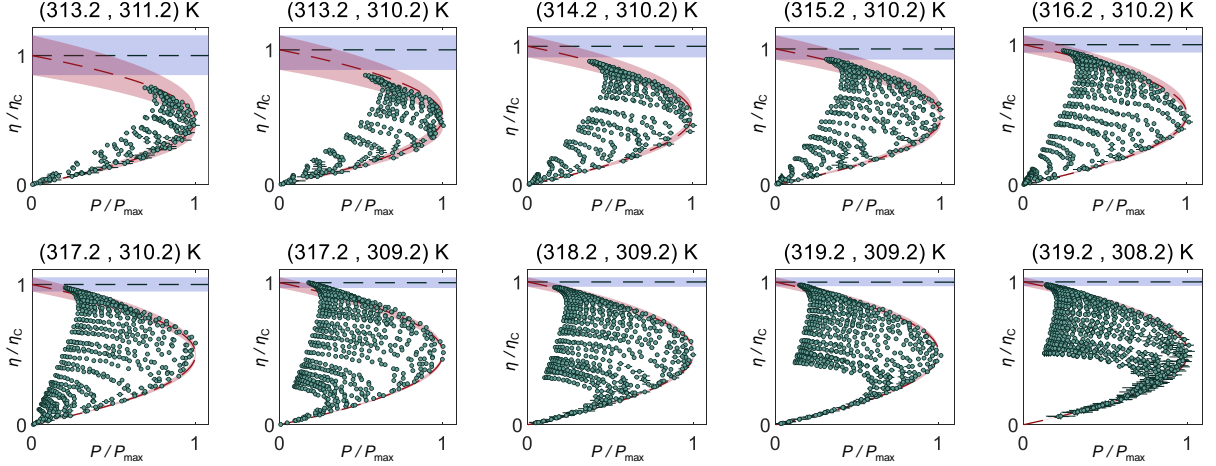


FIG. S3. The $\eta - P$ constraint relation for all the temperature sets measured by the sensor 1 and the strategy to find the efficiency at the maximum power. Cycles with negative output power are not plotted in the above figures.

III. DATA PROCESSING AND DISCUSSION

The heat exchange with the water bath is obtained via calculating the work in the finite-time isothermal expansion and compression processes, i.e,

$$Q_h = -W_{A \rightarrow B' \rightarrow B} = -W_h(\tau_h), \quad (S4)$$

$$Q_c = -W_{C \rightarrow D' \rightarrow D} = -W_c(\tau_c), \quad (S5)$$

where $\tau_h = (L_B - L_A)/v_h + v_h/a_{\max}$ and $\tau_c = (L_C - L_D)/v_c + v_c/a_{\max}$. Trapezoidal integrals is employed to compute the work performed in a single process,

$$W = \sum_i (V_{i+1} - V_i) \frac{p_{i+1} + p_i}{2}, \quad (S6)$$

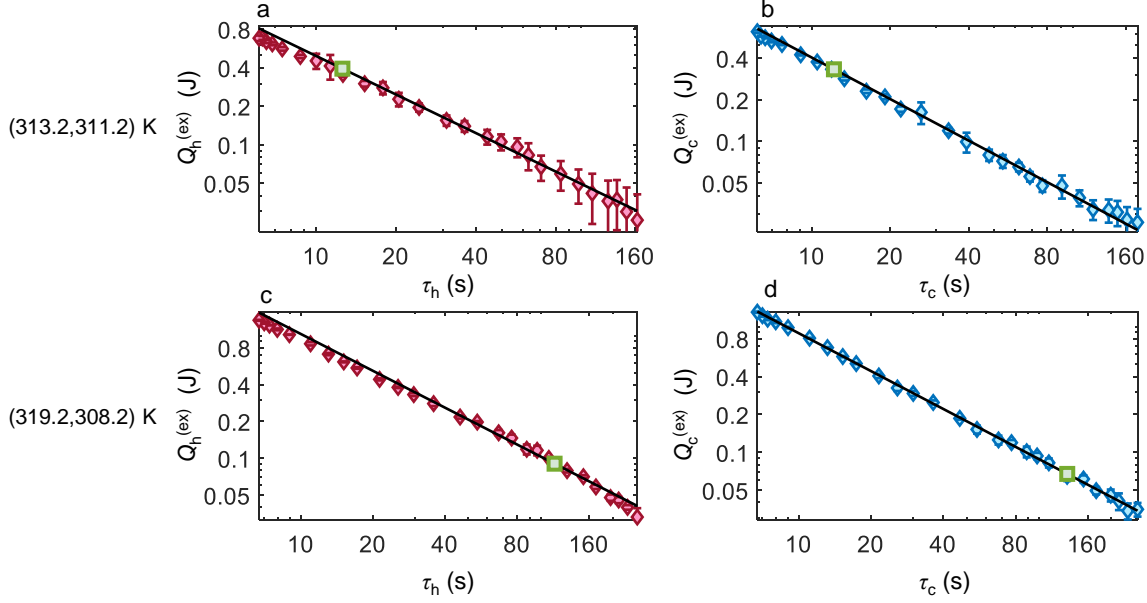


FIG. S4. The $1/\tau$ scaling of the low-dissipation model for the temperature sets (313.2, 311.2) K and (319.2, 308.2) K. The optimal control time (τ_h^* and τ_c^*) is marked with green squares on the figures.

where V_i and p_i are the volume and pressure data points.

The total work extracted is $W_{\text{tot}}(\tau_h, \tau_c) = Q_h + Q_c$ by using the energy conservation law. The power and efficiency are obtained as

$$P(\tau_h, \tau_c) = \frac{W_{\text{tot}}(\tau_h, \tau_c)}{\tau_h + \tau_c}, \quad (\text{S7})$$

$$\eta(\tau_h, \tau_c) = \frac{W_{\text{tot}}(\tau_h, \tau_c)}{Q_h}. \quad (\text{S8})$$

One set of the power-efficiency with temperature combination (319.2, 308.2) K is shown in the main context. We present the scattering plots of the power and the efficiency along with theoretical constraint relations for all the temperature sets in Figure S3. The current data are from the pressure sensor S1. There are 27×27 different combinations of τ_h and τ_c . The data with negative work are neglected in the current plot. The data for all the temperatures fall into the theoretical predictions.

We check the validity of the $1/\tau$ scaling of irreversibility in the low-dissipation model. The irreversibility is measured as the extra heat exchange $Q_{h(c)}^{(\text{ex})} = |Q_{h(c)}(\tau_{h(c)}) - Q_{h(c)}^{(\text{quasi})}|$, where $Q_{h(c)}^{(\text{quasi})}$ is the heat exchange during the quasi-static isothermal processes ($A \rightarrow B$ and $C \rightarrow D$). The extra heat exchange $Q_{h(c)}^{(\text{ex})}$ is plotted as functions of the operation time $\tau_{h(c)}$ in Figure S4 for two temperature sets (313.2, 311.2) K and (319.2, 308.2) K. We mark the optimal operation time τ_h^* and τ_c^* for maximum power on the plot with green squares.

* cpsun@gscaep.ac.cn

† hdong@gscaep.ac.cn

- [1] Van den Broeck, C. Introduction to thermodynamics of irreversible processes. *Phys. Rev. Lett.* **95**, 190602 (2005).
- [2] Esposito, M., Kawai, R., Lindenberg, K. & Van den Broeck, C. Efficiency at maximum power of low-dissipation carnot engines. *Phys. Rev. Lett.* **105**, 150603 (2010).
- [3] Krause, D. E. & Keeley, W. J. Determining the heat capacity ratio of air from almost adiabatic compressions. *Phys. Teach.* **42**, 481–483 (2004).